



Multi-level Monte Carlo weak Galerkin method with nested meshes for stochastic Brinkman problem

Yongle Hao^a, Xiaoshen Wang^b, Kai Zhang^{a,*}

^a Department of Mathematics, Jilin University, Changchun, Jilin 130023, PR China

^b Department of Mathematics and Statistics, University of Arkansas at Little Rock, Little Rock, AR 72204, United States

ARTICLE INFO

Article history:

Received 23 January 2016

Received in revised form 20 June 2017

MSC:

60H35

65N30

65C05

Keywords:

Stochastic Brinkman problem

Multi-level Monte Carlo

Weak Galerkin

ABSTRACT

This paper is devoted to the numerical analysis of a multi-level Monte Carlo weak Galerkin (MLMCWG) approximation with nested meshes for solving stochastic Brinkman equations with two dimensional spatial domain. With weak gradient operator and a stabilizer at hand, the weak Galerkin (WG) technique is a high-order accurate and stable method which can easily handle deterministic partial differential equations with complex geometries, flows with jump fluid viscosity coefficients or high-contrast permeability fields given by each sample. The multi-level Monte Carlo (MLMC) technique with nested meshes balances the sampling error and the spatial approximation error, where the computational cost can be sharply reduced to log-linear complexity with respect to the degree of freedom in spatial direction. The nested meshes requirement is introduced here in order to simplify the analysis, which can be generalized to MLMC with non-nested meshes. Error estimates are derived in terms of the spatial meshsize and the number of samples. The numerical tests are provided to illustrate the behavior of the MLMCWG method and verify our theoretical results regarding optimal convergence of the approximate solutions.

© 2017 Elsevier B.V. All rights reserved.

1. Introduction

There are multitude of interesting models for the mathematical modeling of flows in porous media and materials, e.g., industrial filters, natural water management, dolomite or limestone oil reservoirs, etc.. In these applications, the Darcy model can handle the slow flow problems [1], while it does not predict the cavity problems well. The Stokes model is the steady state of the Navier–Stokes equation, which is capable of modeling flow of cavity problems [2]. The behavior of viscous fluid in cavity and porous media can be captured accurately by the Darcy–Stokes interface model provided the priori information of the interface is given. However, the location and the geometry of the interface are unattainable in many applications, and the interface jump conditions are difficult to impose experimentally even with precise information of the interface at hand. The Brinkman model of porous media, which is a generalization of the Stokes equation and an approximation of the Navier–Stokes equations at low Reynolds numbers, behaves like a Darcy flow and a Stokes flow for the regions with large and small permeability values, respectively [3].

The Brinkman model is a combination of Darcy's and Stokes' equations, which is a very effective model for flows in highly heterogeneous media in real applications. Therefore, the accuracy of the Brinkman flow simulation is of significant practical interest, but it is not easy to design uniform stable efficient algorithms to capture the behavior of the Darcy flow and the Stokes flow in different permeability regions simultaneously. Generally speaking, the usual Darcy stable method does not

* Corresponding author.

E-mail address: kzhang@jlu.edu.cn (K. Zhang).

work well for the Stokes flow and vice versa. The Darcy stable elements, such as the Raviart–Thomas elements, although perform well in the regions with large permeability value, perform poorly in the Stokes regions [4]. On the other hand, the Stokes stable elements, such as the conforming P_2 – P_0 element and the nonconforming Crouzeix–Raviart element, perform well in the regions with small permeability value and perform poorly in the Darcy regions [5]. Many algorithms are proposed by modifying either existing Darcy stable elements or Stokes stable elements to design Brinkman stable elements, which are uniformly stable in both Darcy’s and Stokes’ regions (see [5,6] and references therein). Recently, Mu, Wang, and Ye proposed a weak Galerkin scheme for the deterministic Brinkman equation, which is uniformly stable for large and small permeability regions, based on the weak gradient operator [7]. The most important advantage of this method is that the same formulation works well for both the Darcy and the Stokes problems.

In many practical applications, the interfaces of the Darcy and Stokes domain are unknown beforehand, which is equivalent to that the permeabilities are random variables or the fluid viscosities coefficients jumps stochastically. The stochastic partial differential equation (SPDE) is a powerful tool which adequately describes the behavior of flows in highly heterogeneous media with stochastic permeability and viscosity. Let $D \subset \mathbb{R}^2$ be a bounded convex domain with piecewise smooth boundary and $(\Omega, \mathcal{F}, \mathbb{P})$ be a probability space. Here, we shall consider the following stochastic Brinkman equation: find the velocity $\mathbf{u}(x, \omega) : (\bar{D} \times \Omega)^2 \rightarrow \mathbb{R}^2$ and the pressure $p(x, \omega) : \bar{D} \times \Omega \rightarrow \mathbb{R}$ of the fluid, such that

$$-\mu(\mathbf{x}, \omega)\Delta \mathbf{u} + \nabla p + \mu(\mathbf{x}, \omega)\kappa^{-1}(\mathbf{x}, \omega)\mathbf{u} = \mathbf{f}(\mathbf{x}), \quad \text{in } D \times \Omega, \quad (1)$$

$$\nabla \cdot \mathbf{u} = 0, \quad \text{in } D \times \Omega, \quad (2)$$

$$\mathbf{u} = \mathbf{g}(\mathbf{x}), \quad \text{on } \partial D, \quad (3)$$

where the viscosity μ is a stochastic function with jump and κ is the stochastic permeability tensor (will be specified in the next section). Here the forcing term $\mathbf{f} \in L^2(D)^2$ and the boundary data $\mathbf{g} \in H^{\frac{1}{2}}(\partial D)^2$ are deterministic functions with the compatibility condition

$$\int_{\partial D} \mathbf{g} \cdot \mathbf{n} ds = 0.$$

This type of stochastic problems have many applications in industrial and engineering phenomena, such as groundwater systems [8–10] and vuggy porous media [1,11]. For the sake of simplicity, we consider $\mathbf{g} = 0$ in the sequel.

In this work, we will employ an efficient MLMCWG method for solving stochastic Brinkman equations (1)–(3). There are several merits of our algorithm. As mentioned above, one of the main advantages of the stochastic Brinkman model is that it can capture the Stokes and Darcy type flow behavior depending on the value of κ without priori information of the interface, and the WG method is uniformly stable for Darcy’s and Stokes’ regions for each realization of (1)–(3). Based on weak derivatives [12–15], the WG method shall provide a systematic framework for dealing with high-oscillation or discontinuity of the solutions near the interface of Darcy’s and Stokes’ regions. Secondly, the MLMCWG method requires suboptimal computational cost of log-linear complexity, in terms of the degree of freedom used in the WG approximation. The multi-level Monte Carlo technique has been widely used to replace traditional MC-like methods, so that the computational cost can be sharply reduced [16–19]. Finally, the interfaces between Darcy’s and Stokes’ regions are always complicated, and the traditional triangular partitions may not be suitable for practical computations. On the other hand, the WG method allows arbitrary polygons as long as the partitions are shape regular (cf. [20]) which is more efficient than the standard finite element method (FEM), and the corresponding MLMCWG is superior than MLMCFEM for stochastic case. The convergence analysis of the WG method with different polygons are guaranteed under the same framework, which makes this method more flexible and robust.

The remainder of this paper is organized as follows. In Section 2, the preliminaries including relevant terminologies and notations are presented. In Section 3, we show the weak derivatives, variational formulations, and the weak Galerkin method for the stochastic Brinkman problem. This is followed by the description of the single level Monte Carlo weak Galerkin (SLMCWG) method and the multi level Monte Carlo weak Galerkin method for stochastic Brinkman equations (1)–(3) in Section 3. In Section 4, we present the convergence results of SLMCWG and MLMCWG, respectively. The corresponding computational complexities are also analyzed. In Section 5, several numerical simulations are provided to demonstrate the efficiency of our algorithms. The last section is devoted to some concluding remarks.

2. Preliminaries

2.1. Terminologies

A multi-index $\alpha = (\alpha_1, \alpha_2)$ is a two-tuple of non-negative integers with its length given by $|\alpha| = \alpha_1 + \alpha_2$. For a non-negative integer m , set

$$H^m(D) = \{v \in L^2(D); \partial^\alpha v \in L^2(D), 0 \leq |\alpha| \leq m\}$$

with the generalized higher order derivatives $\partial^\alpha v = \frac{\partial^{\alpha_1 + \alpha_2} v}{\partial x_1^{\alpha_1} \partial x_1^{\alpha_2}}$. The space $H^m(D)$ is equipped with norm and semi-norms defined by

$$\|v\|_{m,X} = \left(\sum_{|\alpha| \leq m} \int_X |\partial^\alpha v|^2 d\mathbf{x} \right)^{\frac{1}{2}} \quad \text{and} \quad |v|_{m,X} = \left(\sum_{|\alpha|=m} \int_X |\partial^\alpha v|^2 d\mathbf{x} \right)^{\frac{1}{2}}.$$

The space $H_0^1(D)$ and $L_0^2(D)$ are defined by

$$H_0^1(D) = \{v \in H^1(D) \mid v = 0 \text{ on } \partial D\}, \quad \text{and} \\ L_0^2(D) = \{v \in H^1(D) \mid \int_D v d\mathbf{x} = 0\}.$$

The space $H(\text{div}; D)$ is defined as the set of vector-valued functions on D given by

$$H(\text{div}; D) = \{\mathbf{v} \mid \mathbf{v} \in [L^2(D)]^2, \nabla \cdot \mathbf{v} \in L^2(D)\}$$

with the norm defined by

$$\|\mathbf{v}\|_{H(\text{div}; D)} = (\|\mathbf{v}\|_{0,D}^2 + \|\nabla \cdot \mathbf{v}\|_{0,D}^2)^{\frac{1}{2}} = (\|\mathbf{v}\|_D^2 + \|\nabla \cdot \mathbf{v}\|_D^2)^{\frac{1}{2}}.$$

The Bochner space $L^p(B; \Omega)$ defined over a product space of the spatial domain and the probability space is the space of strongly measurable functions v ranging in a Banach space B with the norm

$$\|\mathbf{v}\|_{L^p(B; \Omega)} = \left(\int_\Omega \|v(\cdot, \omega)\|_B^p d\mathbb{P}(\omega) \right)^{\frac{1}{p}}, \quad 1 \leq p < \infty, \quad (4)$$

where $\|\cdot\|_B$ is the norm of B .

2.2. Stochastic viscosity and stochastic permeability

Let the domain D be the union of Darcy's region (denoted by D_d) and Stokes' region (denoted by D_s) which have substantially different viscosities $\mu_d > 0$ and $\mu_s > 0$, respectively. The stochastic viscosity $\mu(x, \omega)$ in (1)–(3) is considered as a stochastic jump coefficient and is given by

$$\mu(x, \omega) = \begin{cases} \mu_d, & x \in D_d, \\ \mu_s, & x \in D_s. \end{cases} \quad (5)$$

Many approaches have been proposed to address the problem of simulating two phase random media, and we refer to [21] for more details. Here, we adopt the Lévy processes method to reconstruct two phase composite materials, according to the given samples or given statistical characteristics. We emphasize that the analysis and the algorithm in this paper could be easily extended to the case where $\mu(x, \omega)$ is a uniform positive and bounded function. Next, we will illustrate the motivation and performance of our algorithm.

The stochastic permeability tensor $\kappa(\mathbf{x}, \omega)$ in Eqs. (1)–(3) is uniformly bounded and satisfies uniform elliptic condition, which is equivalent to the existence of constants κ_1 and κ_2 such that

$$\kappa_1 \|\ell\|^2 \leq \sup_{x \in D} |\ell^T \kappa^{-1} \ell| \leq \kappa_2 \|\ell\|^2, \quad \forall \ell \in \mathbb{R}^2 \quad (6)$$

holds for every $\omega \in \Omega$.

3. Weak Galerkin method for stochastic Brinkman problem

In this section, we shall employ the weak Galerkin method for the stochastic Brinkman problem (1)–(3) pathwisely following [7,22], i.e. the deterministic Brinkman equation for each sample $\omega \in \Omega$.

3.1. Variational formulation and weak differential operators

We first introduce the pathwise stochastic variational problem of (1)–(3), which is the foundation of the WG method. The standard pathwise stochastic variational formulation of (1)–(3) is as follows: for a fixed $\omega \in \Omega$, find $(\mathbf{u}, p) \in [L^2(H_0^1(D); \Omega)]^2 \times L^2(L_0^2(D); \Omega)$ such that

$$(\mu(\cdot, \omega) \nabla \mathbf{u}, \nabla \mathbf{v}) + (\mu(\cdot, \omega) \kappa^{-1}(\cdot, \omega) \mathbf{u}, \mathbf{v}) - (\nabla \cdot \mathbf{v}, p) = (\mathbf{f}, \mathbf{v}), \quad (7)$$

$$(\nabla \cdot \mathbf{u}, q) = 0, \quad (8)$$

for all $(\mathbf{v}, q) \in [H_0^1(D)]^2 \times L_0^2(D)$.

Next, we present some terminologies for the weak Galerkin method. Let T_i and T_b be the interior and boundary of the polygonal domain $T \subset \mathbb{R}^2$. The function $v = \{v_i, v_b\}$ is called a stochastic weak function with $v_i \in L^2(L^2(T_i); \Omega)$ and $v_b \in L^2(H^{\frac{1}{2}}(T_b); \Omega)$ with respect to the spatial variables. The space of stochastic weak functions defined on T is given by

$$L^2(W(T); \Omega) = \{v = \{v_i, v_b\} \mid v_i \in L^2(L^2(T_i); \Omega), v_b \in L^2(H^{\frac{1}{2}}(T_b); \Omega)\}. \quad (9)$$

The weak differential operators and its discrete approximations are defined in the following two definitions.

Definition 3.1. Given $\omega \in \Omega$ and $\mathbf{v} \in L^2([W(T)]^2; \Omega)$, the **weak divergence** of $\mathbf{v} = \{\mathbf{v}_i, \mathbf{v}_b\}$ is defined as the linear functional $\nabla_d \cdot \mathbf{v}(\mathbf{x}, \omega)$ on $H^1(T)$, i.e., for any $q \in H^1(T)$,

$$(\nabla_d \cdot \mathbf{v}(\cdot, \omega), q)_T = -(\mathbf{v}_i(\cdot, \omega), \nabla q)_T + \int_{T_b} \mathbf{v}_b(\mathbf{x}, \omega) \cdot \mathbf{n} q ds,$$

where \mathbf{n} is the unit outward normal vector of ∂T . Similarly, the **weak gradient** of \mathbf{v} is defined as the linear functional $\nabla_d \mathbf{v}(\mathbf{x}, \omega)$ on $[H(\text{div}; T)]^{2 \times 2}$, i.e., for any $\mathbf{q} \in [H(\text{div}; T)]^{2 \times 2}$,

$$(\nabla_d \mathbf{v}(\cdot, \omega), \mathbf{q})_T = -(\mathbf{v}_i(\cdot, \omega), \nabla \cdot \mathbf{q})_T + \int_{T_b} \mathbf{v}_b(\mathbf{x}, \omega) \cdot (\mathbf{q} \cdot \mathbf{n}) ds.$$

Definition 3.2. Given $\omega \in \Omega$ and $\mathbf{v} \in L^2([W(T)]^2; \Omega)$, its discrete weak divergence $\nabla_{d,k-1} \cdot \mathbf{v} \in L^2(P_{k-1}(T); \Omega)$ on each T is such that

$$(\nabla_{d,k-1} \cdot \mathbf{v}(\cdot, \omega), q)_T = -(\mathbf{v}_i(\cdot, \omega), \nabla q)_T + \int_{T_b} \mathbf{v}_b(\mathbf{x}, \omega) \cdot \mathbf{n} q ds$$

holds for any $q \in P_{k-1}(T)$. Similarly, its discrete weak gradient $\nabla_{d,k-1} \mathbf{v} \in [L^2(P_{k-1}(T); \Omega)]^{2 \times 2}$ on each T is such that

$$(\nabla_{d,k-1} \mathbf{v}(\cdot, \omega), \mathbf{q})_T = -(\mathbf{v}_i(\cdot, \omega), \nabla \cdot \mathbf{q})_T + \int_{T_b} \mathbf{v}_b(\mathbf{x}, \omega) \cdot (\mathbf{q} \cdot \mathbf{n}) ds$$

holds for any $\mathbf{q} \in [P_{k-1}(T)]^{2 \times 2}$.

For the sake of simplicity, we will drop the subscript $k-1$ in discrete weak gradient $\nabla_{d,k-1}$, and denote it by ∇_d . We also use $(\nabla_d \mathbf{v}(\cdot, \omega), q)_D$ to denote $\sum_{T \in \mathcal{T}_h} (\nabla_d \mathbf{v}(\cdot, \omega), q)_T$, and use similar abbreviations for the discrete weak divergence.

3.2. Weak Galerkin method

Let \mathcal{T}_h be a shape regular triangulation on D with \mathcal{E}_h and $\mathcal{E}_h^i = \mathcal{E}_h \setminus \partial D$ be the set of edges in \mathcal{T}_h and the set of all interior edges, respectively (cf. [13]). For $T \in \mathcal{T}_h$, let h_T denote the maximal diameter of polygons T and $h = \max_{T \in \mathcal{T}_h} h_T$. Define two discrete spaces on spatial domain D by

$$U_h(D) = \{\mathbf{v} = \{\mathbf{v}_i, \mathbf{v}_b\} \mid \mathbf{v}_i|_T \in [P_k(T_i)]^2, \mathbf{v}_b|_T \in [P_k(T_b)]^2, \\ \forall T \in \mathcal{T}_h, \mathbf{v}_b = \mathbf{0} \text{ on } \partial D\},$$

$$P_h(D) = \{q \in L_0^2(D) \mid q|_T \in P_{k-1}(T), \forall T \in \mathcal{T}_h\},$$

then the two stochastic weak Galerkin spaces U_h and P_h for the velocity and pressure, respectively, are given by

$$U_h = L^2(U_h(D); \Omega) = \{\mathbf{v} = \{\mathbf{v}_i, \mathbf{v}_b\} \mid \mathbf{v}_i|_T \in L^2([P_k(T_i)]^2; \Omega), \\ \mathbf{v}_b|_T \in L^2([P_k(T_b)]^2; \Omega), \forall T \in \mathcal{T}_h, \mathbf{v}_b = \mathbf{0} \text{ on } \partial D\}, \\ P_h = L^2(P_h(D); \Omega) = \{q \in L^2(L_0^2(D); \Omega) \mid q|_T \in L^2(P_{k-1}(T); \Omega), \forall T \in \mathcal{T}_h\}.$$

For each realization $\omega \in \Omega$, we introduce the following bilinear forms:

$$a(\mathbf{u}, \mathbf{v}; \omega) = (\mu(\cdot, \omega) \nabla_d \mathbf{u}(\cdot, \omega), \nabla_d \mathbf{v})_D + (\mu(\cdot, \omega) \kappa^{-1}(\cdot, \omega) \mathbf{u}(\cdot, \omega), \mathbf{v})_D, \\ s(\mathbf{u}, \mathbf{v}; \omega) = \sum_{T \in \mathcal{T}_h} h_T^{-1} \langle R_b(\mathbf{u}_i(\mathbf{x}, \omega)) - \mathbf{u}_b(\mathbf{x}, \omega), R_b(\mathbf{v}_i(\mathbf{x})) - \mathbf{v}_b(\mathbf{x}) \rangle_{L^2(T_b)}, \\ a_1(\mathbf{u}, \mathbf{v}; \omega) = a(\mathbf{u}, \mathbf{v}; \omega) + s(\mathbf{u}, \mathbf{v}; \omega), \\ b_1(\mathbf{v}, p; \omega) = (\nabla_d \cdot \mathbf{v}, p(\cdot, \omega))_D, \quad b_2(\mathbf{u}, q; \omega) = (\nabla_d \cdot \mathbf{u}(\cdot, \omega), q)_D,$$

for $\mathbf{u} \in U_h, p \in P_h, \mathbf{v} \in U_h(D)$, and $q \in P_h(D)$. Here, the operator R_b is the standard L^2 projection from $[H^1(T)]^2$ onto $[H^{\frac{1}{2}}(T_b)]^2$.

Now, we are at the stage to propose the pathwise weak Galerkin scheme for (1)–(3).

Pathwise weak Galerkin scheme: Seeking $u_h = \{u_{hi}, u_{hb}\} \in U_h$ and $p_h \in P_h$, for each realization $\omega \in \Omega$, such that

$$a_1(\mathbf{u}_h, \mathbf{v}_h; \omega) - b_1(\mathbf{v}_h, p_h; \omega) = (\mathbf{f}, \mathbf{v}_{0h}), \quad \forall \mathbf{v}_h = \{\mathbf{v}_{hi}, \mathbf{v}_{hb}\} \in U_{Dh}, \quad (10)$$

$$b_2(\mathbf{u}_h, q_h; \omega) = 0, \quad \forall q_h \in P_{Dh}. \quad (11)$$

Furthermore, let

$$a_3(\mathbf{u}, \mathbf{v}; \omega) = a(\mathbf{u}, \mathbf{v}; \omega) + s(\mathbf{u}, \mathbf{v}; \omega), \quad b_3(\mathbf{v}, p; \omega) = (\nabla_d \cdot \mathbf{v}(\cdot, \omega), p(\cdot, \omega))_D,$$

for $\mathbf{u}, \mathbf{v} \in U_h$ and $p \in P_h$, then the weak Galerkin scheme for (1)–(3) is given by

Weak Galerkin scheme: Find $u_h = \{u_{hi}, u_{hb}\} \in U_h$ and $p_h \in P_h$, such

$$\bar{a}_3(\mathbf{u}_h, \mathbf{v}_h) - \bar{b}_3(\mathbf{v}_h, p_h) = (\mathbf{f}, \mathbf{v}_{hi}), \quad \forall \mathbf{v}_h = \{\mathbf{v}_{hi}, \mathbf{v}_{hb}\} \in U_h, \quad (12)$$

$$\bar{b}_3(\mathbf{u}_h, q_h) = 0, \quad \forall q_h \in P_h, \quad (13)$$

where

$$\bar{a}_3(\mathbf{u}, \mathbf{v}) = \mathbb{E}[a_3(\mathbf{u}, \mathbf{v}; \omega)], \quad \bar{b}_3(\mathbf{v}, p) = \mathbb{E}[b_3(\mathbf{v}, p; \omega)]$$

with \mathbb{E} denoting the expectation with respect to the probability measure \mathbb{P} .

3.3. Estimates for weak Galerkin method

Before presenting the estimates for the weak Galerkin method, we introduce some useful norms. Given $\omega \in \Omega, \forall \mathbf{v} \in U_h$, define

$$\|\mathbf{v}(\cdot, \omega)\| = (a_1(\mathbf{v}(\cdot, \omega), \mathbf{v}(\cdot, \omega)))^{\frac{1}{2}} \quad (14)$$

for the velocity space. For the pressure space, given $\omega \in \Omega, \forall q \in P_h$, we define

$$|q(\cdot, \omega)|_1^2 = \sum_{T \in \mathcal{T}_h} \|\nabla q(\cdot, \omega)\|_T^2 + h^{-1} \sum_{e \in \mathcal{E}_h^0} \|[q(\cdot, \omega)]\|_e^2,$$

where $[q]$ is the jump of the function q across e . In the sequel, we will use

$$\|\mathbf{v}\|_{L^2(U_h(D); \Omega)}^2 = \mathbb{E}[\|\mathbf{v}\|^2], \quad \text{for any } \mathbf{v} \in U_h, \quad (15)$$

$$|q|_{L^2(P_h(D); \Omega)}^2 = \mathbb{E}[|q|_1^2], \quad \text{for any } q \in P_h. \quad (16)$$

Recall that the stochastic viscosity $\mu(x, \omega)$ specified in (5) is positive and bounded, and the stochastic permeability tensor $\kappa(\mathbf{x}, \omega)$ specified in (6) is a positive definite matrix and is bounded, the following estimate for pathwise weak Galerkin scheme (10)–(11) follows from similar arguments as in Theorem 6.1 of [7].

Lemma 3.3. Let $(\mathbf{u}, p) \in L^2([H_0^1(D) \cap H^{k+1}(D)]^2; \Omega) \times L^2([L_0^2(D) \cap H^k(D)]; \Omega)$ with $k \geq 1$ and $(\mathbf{u}_h, p_h) \in U_h \times P_h$ be the solutions of (1)–(3) and the weak Galerkin solution of (12)–(13), respectively. Then, for any given $\omega \in \Omega$, we have

$$\|\mathbf{u}(\cdot, \omega) - \mathbf{u}_h(\cdot, \omega)\| + h|p(\cdot, \omega) - p_h(\cdot, \omega)|_1 \leq Ch^k(\|\mathbf{u}(\cdot, \omega)\|_{k+1, D} + \|p(\cdot, \omega)\|_{k, D}).$$

Furthermore, we have

$$\|\mathbf{u} - \mathbf{u}_h\|_{L^2(U_h(D); \Omega)} + h|p - p_h|_{L^2(P_h(D); \Omega)} \leq Ch^k(\|\mathbf{u}\|_{L^2(H^{k+1}(D); \Omega)} + \|p\|_{L^2(H^k(D); \Omega)}). \quad (17)$$

For the weak Galerkin scheme (12)–(13), we have the following stability estimate.

Lemma 3.4. The weak Galerkin scheme (12)–(13) admits a unique solution $(\mathbf{u}_h, p_h) \in U_h \times P_h$. Furthermore, we have

$$\|\mathbf{u}_h\|_{L^2(U_h(D); \Omega)} \leq C\|\mathbf{f}\|_{0, D}, \quad (18)$$

where C is a constant.

Proof. Set $\mathbf{v}_h = \mathbf{u}_h$ and $q_h = p_h$ in (12)–(13), we obtain

$$\bar{b}_3(\mathbf{u}_h, p_h) = 0, \quad \text{and} \quad \mathbb{E}[\|\mathbf{u}_h\|^2] = \mathbb{E}[(\mathbf{f}, \mathbf{u}_{hi})].$$

Together with the definitions (14), (15), and Hölder inequality, we have

$$\begin{aligned} \|\mathbf{u}_h\|_{L^2(U_h(D); \Omega)}^2 &= \mathbb{E}[\|\mathbf{u}_h\|^2] = \mathbb{E}[(\mathbf{f}, \mathbf{u}_{hi})] \\ &\leq C\|\mathbf{f}\|_{0, D} \mathbb{E}[\|\mathbf{u}_{hi}\|_{0, D}^2]^{\frac{1}{2}} \\ &\leq C\|\mathbf{f}\|_{0, D} \|\mathbf{u}_h\|_{L^2(U_h(D); \Omega)}, \end{aligned}$$

which implies the estimate (18).

In order to show the uniqueness, we set $\mathbf{f} = 0$ in (12). It follows from (18) that $\mathbf{u}_h = 0$ and

$$\bar{b}_3(\mathbf{v}_h, p_h) = 0, \quad \forall \mathbf{v}_h = \{\mathbf{v}_{hi}, \mathbf{v}_{hb}\} \in U_h. \quad (19)$$

Let $\mathbf{v}_h = F(p_h) \in U_h$ be the numerical flux of p_h in (19). Using the Lemma 3.2 in [7] we obtain

$$0 = \bar{b}_3(F(p_h), p_h) = |p_h|_{L^2(p_h(D); \Omega)}^2.$$

It follows from $p_h \in L_0^2(D)$ that $p_h = 0$. This completes the proof. \square

4. Monte Carlo weak Galerkin method

In this section, we introduce the single level Monte Carlo weak Galerkin (SLMCWG) method for solving stochastic Brinkman equations (1)–(3), which is a combination of the Monte Carlo method for stochastic domain and the Weak Galerkin method for spatial domain. Based on the estimate of the SLMCWG method and nested meshes, we also present an efficient MLMCWG method.

4.1. Single level Monte Carlo weak Galerkin method

For the stochastic Brinkman equations (1)–(3), we are interested in the statistic quantity of $(\mathbf{u}, p) \in L^2([H_0^1(D) \cap H^{k+1}(D)]^2; \Omega) \times L^2([L_0^2(D) \cap H^k(D)]; \Omega)$. To obtain the expectation, we select M_1 independent, identically distributed realizations of the stochastic viscosity $\mu(\mathbf{x}, \omega)$ and stochastic permeability $\kappa(\mathbf{x}, \omega)$. Denote by $(\mathbf{u}_h(\cdot, \omega_i), p_h(\cdot, \omega_i)) \in U_h(D) \times P_h(D)$, $i = 1, 2, \dots, M_1$ the realizations of numerical solution of Eqs. (1)–(3) corresponding to the sample ω_i . Let

$$E_{M_1}[\mathbf{u}_h] := \frac{1}{M_1} \sum_{i=1}^{M_1} \mathbf{u}_h(\mathbf{x}, \omega_i) \quad \text{and} \quad E_{M_1}[p_h] := \frac{1}{M_1} \sum_{i=1}^{M_1} p_h(\mathbf{x}, \omega_i). \quad (20)$$

It follows from the law of large numbers that

$$\lim_{M_1 \rightarrow \infty} \mathbb{E}[(\mathbb{E}[\mathbf{u}_h] - E_{M_1}[\mathbf{u}_h])] = 0 \quad \text{and} \quad \lim_{M_1 \rightarrow \infty} \mathbb{E}[(\mathbb{E}[p_h] - E_{M_1}[p_h])] = 0. \quad (21)$$

By Definitions 3.1 and 3.2, we can easily deduce the following identity which is necessary for the convergence analysis (see Lemma 4.1 in [22]).

Lemma 4.1. For any $\mathbf{v} \in L^2(U_h(D); \Omega)$, we have

$$\mathbb{E}[a_3(\mathbb{E}[\mathbf{v}], \mathbf{v})] = a_3(\mathbb{E}[\mathbf{v}], \mathbb{E}[\mathbf{v}]), \quad \forall \mathbf{v} \in L^2(U_h(D); \Omega). \quad (22)$$

Now, we are in the position to describe the exact convergence rate of the sequences $\{E_M[\mathbf{u}_h]\}$ and $\{E_M[p_h]\}$ by using Lemma 4.1 and standard MC analysis [23,24].

Lemma 4.2. For any positive integer M_1 , we have

$$\|\mathbb{E}[\mathbf{v}] - E_{M_1}[\mathbf{v}]\|_{L^2(U_h(D); \Omega)} \leq \frac{1}{\sqrt{M_1}} \|\mathbf{v}\|_{L^2(U_h(D); \Omega)}, \quad \forall \mathbf{v} \in L^2(U_h(D); \Omega), \quad (23)$$

$$|\mathbb{E}[q] - E_{M_1}[q]|_{L^2(P_h(D); \Omega)} \leq \frac{1}{\sqrt{M_1}} \|q\|_{L^2(P_h(D); \Omega)}, \quad \forall q \in L^2(P_h(D); \Omega). \quad (24)$$

Proof. For the completeness, we give the details here. By using the definition of $\|\cdot\|$, and the fact that the $\mathbf{v}(\mathbf{x}, \omega_i)$'s are independent and have the same expectation $\mathbb{E}[\mathbf{v}(\mathbf{x}, \cdot)]$, we obtain

$$\begin{aligned} \|\mathbb{E}[\mathbf{v}] - E_{M_1}[\mathbf{v}]\|_{L^2(U_h(D); \Omega)}^2 &= \mathbb{E}\left[\left\|\mathbb{E}[\mathbf{v}] - \frac{1}{M_1} \sum_{i=1}^{M_1} \mathbf{v}(\cdot, \omega_i)\right\|^2\right] \\ &= \mathbb{E}\left[\left\|\frac{1}{M_1} \sum_{i=1}^{M_1} [\mathbb{E}[\mathbf{v}] - \mathbf{v}(\cdot, \omega_i)]\right\|^2\right] \leq \frac{1}{M_1} \mathbb{E}[\|\mathbb{E}[\mathbf{v}] - \mathbf{v}\|^2] \\ &= \frac{1}{M_1} (\mathbb{E}[\|\mathbf{v}\|^2] - \|\mathbb{E}[\mathbf{v}]\|^2) \leq \frac{1}{M_1} \|\mathbf{v}\|_{L^2(U_h(D); \Omega)}^2. \end{aligned}$$

The second last equality follows from the identity (22). Similarly, we can obtain the estimate (24). \square

4.2. Multi-level Monte Carlo weak Galerkin method

Let $\{\mathcal{T}_{h_n}\}_{n=1}^N$ be the nested shape regular triangulations of D with the meshsize $h_n = \max_{T \in \mathcal{T}_n} h_T$. Denote by $U_{h_n} \times P_{h_n}$ the weak Galerkin spaces at n th level spatial domain with meshsize h_n , and $(\mathbf{u}_{h_n}, p_{h_n})$ denotes the corresponding WG solution.

For $T^n \in \mathcal{T}_{h_n}$, $T^{n+1} \in \mathcal{T}_{h_{n+1}}$ with $T^{n+1} \subset T^n$, and $\mathbf{v} \in U_{h_n}$, if we identify \mathbf{v} with $\hat{\mathbf{v}} = \{\hat{\mathbf{v}}_i, \hat{\mathbf{v}}_b\} \in U_{h_{n+1}}$, where $\hat{\mathbf{v}}_i = \mathbf{v}_i$ on T_i^{n+1} and $\hat{\mathbf{v}}_b = \mathbf{v}_i|_{\partial T^{n+1} \setminus \partial T^n}$, then we have

$$U_{h_1}(D) \subset \cdots \subset U_{h_n}(D) \subset \cdots \subset U_{h_N}(D) \text{ and } U_{h_1} \subset \cdots \subset U_{h_n} \subset \cdots \subset U_{h_N}.$$

Similarly, we have

$$P_{h_1}(D) \subset \cdots \subset P_{h_n}(D) \subset \cdots \subset P_{h_N}(D) \text{ and } P_{h_1} \subset \cdots \subset P_{h_n} \subset \cdots \subset P_{h_N}$$

for the discrete pressure spaces. For the purpose of illustration, we assume $h_n = h_{n-1}/2$ for $l = 2, \dots, N$.

Setting $\mathbf{u}_{h_0} = 0$ and $p_{h_0} = 0$, we can obtain

$$\mathbf{u}_{h_N} = \sum_{n=1}^N (\mathbf{u}_{h_n} - \mathbf{u}_{h_{n-1}}) \quad \text{and} \quad p_{h_N} = \sum_{n=1}^N (p_{h_n} - p_{h_{n-1}}).$$

Together with the linearity of expectation, yields

$$\mathbb{E}[\mathbf{u}_{h_N}(x, \cdot)] = \sum_{n=1}^N (\mathbb{E}[\mathbf{u}_{h_n}(x, \cdot)] - \mathbb{E}[\mathbf{u}_{h_{n-1}}(x, \cdot)]), \quad (25)$$

$$\mathbb{E}[p_{h_N}(x, \cdot)] = \sum_{n=1}^N (\mathbb{E}[p_{h_n}(x, \cdot)] - \mathbb{E}[p_{h_{n-1}}(x, \cdot)]). \quad (26)$$

Taking advantage of the law of large numbers (21) and the last two identities, we can approximate the quantities $\mathbb{E}[\mathbf{u}_{h_N}]$ and $\mathbb{E}[p_{h_N}]$ by

$$\mathbb{E}[\mathbf{u}_{h_N}] \approx E_{M_N}^N[\mathbf{u}_{h_N}(x, \omega)] = \sum_{n=1}^N (E_{M_n}[\mathbf{u}_{h_n}(x, \omega)] - E_{M_{n-1}}[\mathbf{u}_{h_{n-1}}(x, \omega)]), \quad (27)$$

and

$$\mathbb{E}[p_{h_N}] \approx E_{M_N}^N[p_{h_N}(x, \omega)] = \sum_{n=1}^N (E_{M_n}[p_{h_n}(x, \omega)] - E_{M_{n-1}}[p_{h_{n-1}}(x, \omega)]), \quad (28)$$

respectively, where M_n denotes the number of samples at the n th level.

Now, we are at the stage to present the H^1 -like convergence result of the MLMCWG method.

Theorem 4.3. Let $(\mathbf{u}, p) \in L^2([H_0^1(D) \cap H^{k+1}(D)]^2; \Omega) \times L^2([L_0^2(D) \cap H^k(D)]; \Omega)$ and $(\mathbf{u}_{h_N}, p_{h_N}) \in U_{h_N} \times P_{h_N}$ be the solutions of (1)–(3) and the MLMCWG method, respectively. Then, we have the following error estimate for the MLMCWG method

$$\begin{aligned} & \| \mathbb{E}[\mathbf{u}] - E_{M_N}^N[\mathbf{u}_{h_N}] \|_{L^2(U_{h_N}(D); \Omega)} + h_N \| \mathbb{E}[p] - E_{M_N}^N[p_{h_N}] \|_{L^2(P_{h_N}(D); \Omega)} \\ & \leq C \left(h_N^k + \sum_{n=1}^N h_n^k M_n^{-\frac{1}{2}} \right) (\| \mathbf{u} \|_{L^2(H^{k+1}(D); \Omega)} + \| p \|_{L^2(H^k(D); \Omega)}), \end{aligned} \quad (29)$$

where the constant C is independent of h_n and M_n .

Proof. We only prove the estimate (29) for the velocity here, and the similar result holds for pressure. It follows from the triangle inequality that

$$\begin{aligned} & \| \mathbb{E}[\mathbf{u}] - E_{M_N}^N[\mathbf{u}_{h_N}] \|_{L^2(U_{h_N}(D); \Omega)} \\ & \leq \| \mathbb{E}[\mathbf{u}] - \mathbb{E}[\mathbf{u}_{h_N}] \|_{L^2(U_{h_N}(D); \Omega)} + \| \mathbb{E}[\mathbf{u}_{h_N}] - E_{M_N}^N[\mathbf{u}_{h_N}] \|_{L^2(U_{h_N}(D); \Omega)}, \\ & := I_1 + I_2. \end{aligned} \quad (30)$$

Using the linearity of expectation in estimate (17) and the definitions (14)–(15), we obtain

$$\begin{aligned} I_1 & = \| \mathbb{E}[\mathbf{u}] - \mathbb{E}[\mathbf{u}_{h_N}] \|_{L^2(U_{h_N}(D); \Omega)} \\ & \leq Ch_N^k (\| \mathbf{u} \|_{L^2(H^{k+1}(D); \Omega)} + \| p \|_{L^2(H^k(D); \Omega)}). \end{aligned} \quad (31)$$

For any $\mathbf{v} \in L^2(U_{h_{n-1}}(D); \Omega) \subset L^2(U_{h_n}(D); \Omega)$, it is obvious that

$$\|\mathbf{v}\|_{L^2(U_{h_n}(D); \Omega)} \leq \|\mathbf{v}\|_{L^2(U_{h_{n-1}}(D); \Omega)}. \quad (32)$$

Then for the term I_2 , we have

$$\begin{aligned} I_2 &= \|\mathbb{E}[\mathbf{u}_{h_N}] - E_{M_N}^N[\mathbf{u}_{h_N}]\|_{L^2(U_{h_N}(D); \Omega)} \\ &\leq \left\| \sum_{n=1}^N (\mathbb{E}[\mathbf{u}_{h_n} - \mathbf{u}_{h_{n-1}}] - E_{M_n}^n[\mathbf{u}_{h_n} - \mathbf{u}_{h_{n-1}}]) \right\|_{L^2(U_{h_N}(D); \Omega)}, \\ &\leq \sum_{n=1}^N \|\mathbb{E}[\mathbf{u}_{h_n} - \mathbf{u}_{h_{n-1}}] - E_{M_n}^n[\mathbf{u}_{h_n} - \mathbf{u}_{h_{n-1}}]\|_{L^2(U_{h_n}(D); \Omega)}. \end{aligned}$$

For each $n = 1, \dots, N$ in the above inequality, by using Lemma 4.2, the triangle inequality, and error estimate (17), we have

$$\begin{aligned} &\|\mathbb{E}[\mathbf{u}_{h_n} - \mathbf{u}_{h_{n-1}}] - E_{M_n}^n[\mathbf{u}_{h_n} - \mathbf{u}_{h_{n-1}}]\|_{L^2(U_{h_n}(D); \Omega)} \\ &= \|(\mathbb{E} - E_{M_n}^n)(\mathbf{u}_{h_n} - \mathbf{u}_{h_{n-1}})\|_{L^2(U_{h_n}(D); \Omega)} \\ &\leq \frac{1}{\sqrt{M_n}} \|\mathbf{u}_{h_n} - \mathbf{u}_{h_{n-1}}\|_{L^2(U_{h_n}(D); \Omega)} \\ &\leq \frac{1}{\sqrt{M_n}} (\|\mathbf{u} - \mathbf{u}_{h_n}\|_{L^2(U_{h_n}(D); \Omega)} + \|\mathbf{u} - \mathbf{u}_{h_{n-1}}\|_{L^2(U_{h_{n-1}}(D); \Omega)}) \\ &\leq C \frac{h_n^k + h_{n-1}^k}{\sqrt{M_n}} (\|\mathbf{u}\|_{L^2(H^{k+1}(D); \Omega)} + \|p\|_{L^2(H^k(D); \Omega)}) \\ &\leq Ch_n^k M_n^{-\frac{1}{2}} (\|\mathbf{u}\|_{L^2(H^{k+1}(D); \Omega)} + \|p\|_{L^2(H^k(D); \Omega)}). \end{aligned}$$

By summing up the above inequalities for n from 1 to N , we have

$$I_2 \leq C \sum_{n=1}^N h_n M_n^{-\frac{1}{2}} (\|\mathbf{u}\|_{L^2(H^{k+1}(D); \Omega)} + \|p\|_{L^2(H^k(D); \Omega)}). \quad (33)$$

(33) together with the estimates (30) and (31) implies the conclusion (29) for the velocity. This completes the proof. \square

By using a duality argument as in [13], we have the following L^2 -like convergence estimate without proof.

Proposition 4.4. Let $(\mathbf{u}, p) \in L^2([H_0^1(D) \cap H^{k+1}(D)]^2; \Omega) \times L^2((L_0^2(D) \cap H^k(D)); \Omega)$ and $(\mathbf{u}_{h_N}, p_{h_N}) \in U_{h_N} \times P_{h_N}$ be the solutions of (1)–(3) and the MLMCWG method, respectively. Then, we have the following error estimate for the MLMCWG method

$$\begin{aligned} &\|\mathbb{E}[\mathbf{u}] - E_{M_N}^N[\mathbf{u}_{h_N}]\|_{L^2(U_{h_N}(D); \Omega)} + h_N \|\mathbb{E}[p] - E_{M_N}^N[p_{h_N}]\|_{L^2(P_{h_N}(D); \Omega)} \\ &\leq C \left(h_N^{k+1} + \sum_{n=1}^N h_n^{k+1} M_n^{-\frac{1}{2}} \right) (\|\mathbf{u}\|_{L^2(H^{k+1}(D); \Omega)} + \|p\|_{L^2(H^k(D); \Omega)}), \end{aligned} \quad (34)$$

where the constant C is independent of h_n and M_n .

Remark 4.5. In order to balance the Multi-level Monte Carlo error and the WG discretization errors in (29) and (34) for the MLMCWG method, we adopt the optimal realizations of PDEs at each level as

$$M_n = O(n^{2+2\varepsilon} 2^{2(N-n)}), \quad n = 1, 2, \dots, N \quad (35)$$

with $\varepsilon > 0$ is an arbitrarily small number (cf. [16]). With this choice, the estimates (29) and (34) can be simplified as

$$\begin{aligned} &\|\mathbb{E}[\mathbf{u}] - E_{M_N}^N[\mathbf{u}_{h_N}]\|_{L^2(U_{h_N}(D); \Omega)} + h_N \|\mathbb{E}[p] - E_{M_N}^N[p_{h_N}]\|_{L^2(P_{h_N}(D); \Omega)} \\ &\leq Ch_N^k (\|\mathbf{u}\|_{L^2(H^{k+1}(D); \Omega)} + \|p\|_{L^2(H^k(D); \Omega)}), \end{aligned} \quad (36)$$

$$\begin{aligned} &\|\mathbb{E}[\mathbf{u}] - E_{M_N}^N[\mathbf{u}_{h_N}]\|_{L^2(U_{h_N}(D); \Omega)} + h_N \|\mathbb{E}[p] - E_{M_N}^N[p_{h_N}]\|_{L^2(P_{h_N}(D); \Omega)} \\ &\leq Ch_N^{k+1} (\|\mathbf{u}\|_{L^2(H^{k+1}(D); \Omega)} + \|p\|_{L^2(H^k(D); \Omega)}). \end{aligned} \quad (37)$$

Table 1

The convergence rates of Raviart–Thomas element and conforming P_2 – P_0 element for deterministic Brinkman equation with $a = 1$ and $a = 10^4$ in Example 5.1.

h	Raviart–Thomas element				P_2 – P_0 element			
	$a = 1$		$a = 10^4$		$a = 1$		$a = 10^4$	
	$\ e_{\mathbf{u}h}\ $	Rate	$\ e_{\mathbf{u}h}\ $	Rate	$\ e_{\mathbf{u}h}\ $	Rate	$\ e_{\mathbf{u}h}\ $	Rate
1/4	0.2752	–	0.2391	–	0.2436	–	0.2817	–
1/8	0.1592	0.79	0.0668	1.84	0.0564	2.11	0.1218	1.21
1/16	0.0877	0.86	0.0180	1.89	0.0137	2.04	0.0553	1.14
1/32	0.0463	0.92	0.0047	1.94	0.0035	1.98	0.0272	1.02
1/64	0.0229	1.02	0.0012	1.98	0.0009	2.01	0.0139	0.97

The total computational complexity is given by

$$\text{Cost}(N) = CD_N(\log D_N)^{3+\varepsilon},$$

where D_N is the degree of freedom of the weak Galerkin discretization on N th spatial level.

5. Numerical simulations

In this section, we present the results of several numerical simulations to verify the convergence results in the previous section, and the efficiency of the weak Galerkin method. Consider the stochastic partial differential equations (1)–(3) with the stochastic velocity $\mathbf{u}(x, \xi)$ and the stochastic pressure $p(x, \xi)$ in $D = [0, 1] \times [0, 1] \subset \mathbb{R}^2$. All these experiments have been implemented on a high-performance computer, Inspur TS10000 with 12 cores.

For any given $\omega \in \Omega$, the errors of pathwise weak Galerkin scheme (10)–(11) for the stochastic Brinkman equations are measured by the following norms:

$$\begin{aligned} \|\mathbf{v}(\cdot, \omega)\|^2 &= a_1(\mathbf{v}(\cdot, \omega), \mathbf{v}(\cdot, \omega)), \\ \|\mathbf{v}(\cdot, \omega)\|^2 &= \sum_{T \in \mathcal{T}_h} \int_T |\mathbf{v}_i(\mathbf{x}, \omega)|^2 d\mathbf{x}, \\ \|q(\cdot, \omega)\|^2 &= \sum_{T \in \mathcal{T}_h} \int_T |q(\mathbf{x}, \omega)|^2 d\mathbf{x}, \end{aligned}$$

where the first norm is a discrete H^1 norm, and the last two norms are L^2 -norms for velocity and pressure, respectively. We shall also evaluate

$$\begin{aligned} \|\mathbf{v}\|_{L^2(U_h(D); \Omega)}^2 &= \mathbb{E}_M[\|\mathbf{v}\|^2], \\ \|\mathbf{v}\|_{L^2(U_h(D); \Omega)}^2 &= \mathbb{E}_M[\|\mathbf{v}\|^2], \\ \|q\|_{L^2(P_h(D); \Omega)}^2 &= \mathbb{E}_M[\|q\|^2], \end{aligned}$$

to check error estimates for the MLMCWG method.

Example 5.1. This example is taken from [4,25] with constant viscosity $\mu = 1$ and the deterministic permeability is given by

$$\kappa^{-1} = a(\cos 2\pi x_2 + 1.1),$$

where a is a given constant. The geometry of κ^{-1} is given by Fig. 1. Let

$$\begin{aligned} \mathbf{f} &= (\sin(2\pi x_1) \cos(2\pi x_2), -\cos(2\pi x_1) \sin(2\pi x_2))^T, \\ \mathbf{g} &= (\sin(2\pi x_1) \cos(2\pi x_2), -\cos(2\pi x_1) \sin(2\pi x_2))^T. \end{aligned}$$

The corresponding exact solution is given by

$$\mathbf{u} = (\sin(2\pi x_1) \cos(2\pi x_2), -\cos(2\pi x_1) \sin(2\pi x_2))^T \quad \text{and} \quad p = x_1^2 x_2^2 - \frac{1}{9}.$$

It is easy to check that $\nabla \cdot \mathbf{u} = 0$ and $\int_D p = 0$. In order to check the convergence results of Lemma 3.3 numerically, we first use the Raviart–Thomas element (Darcy stable element), the conforming P_2 – P_0 element (Stokes stable element), and the weak Galerkin method for solving this deterministic Brinkman equation.

The computational domain D is triangulated by the uniform triangles. Denote $e_{\mathbf{u}h} = \mathbf{u} - \mathbf{u}_h$ and $e_{ph} = p - p_h$. Table 1 shows the convergence results of lowest order Raviart–Thomas element and conforming P_2 – P_0 element as the mesh size h

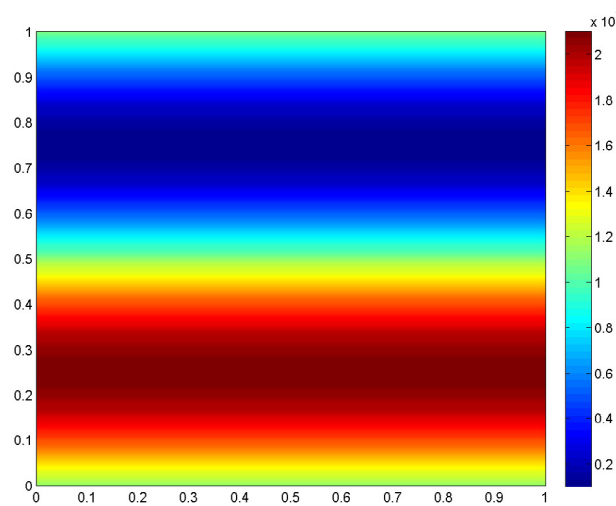


Fig. 1. Geometry of κ^{-1} in Example 5.1 with $a = 10^4$.

Table 2

The convergence rates of WG method for deterministic Brinkman equation with $a = 1$ in Example 5.1.

h	$\ e_{uh}\ $	Rate	$\ e_{uh}\ $	Rate	$\ e_{ph}\ $	Rate
1/4	5.1983	–	0.9215	–	0.5112	–
1/8	2.8220	0.88	0.1868	2.30	0.2952	0.79
1/16	1.4417	0.97	0.0425	2.13	0.1470	1.01
1/32	0.7248	0.99	0.0103	2.04	0.0730	1.01
1/64	0.3629	0.99	0.0026	2.01	0.0364	1.00

Table 3

The convergence rates of WG method for deterministic Brinkman equation with $a = 10^4$ in Example 5.1.

h	$\ e_{uh}\ $	Rate	$\ e_{uh}\ $	Rate	$\ e_{ph}\ $	Rate
1/4	4.2007	–	0.5536	–	1.4931	–
1/8	3.3522	0.33	0.2267	1.29	1.0313	0.53
1/16	2.3189	0.53	0.0831	1.45	0.5570	0.89
1/32	1.3973	0.73	0.0252	1.72	0.2837	0.97
1/64	0.6605	1.08	0.0057	2.14	0.1271	1.16

refining. We see from the third and fifth columns that the L^2 -convergence rate for \mathbf{u} by using the Raviart–Thomas element is two in case of $a = 10^4$ (large permeability) as expected, while the convergence rate for the velocity \mathbf{u} is decreased to one in case $a = 1$ (small permeability). On the other hand, the convergence rate of the conforming P_2 – P_0 element for the velocity \mathbf{u} is decreased to one (the ninth column) in case of large permeability. These phenomena are consistent with the computational results in [4], which verify that the Raviart–Thomas element performs well only in the Darcy region while the conforming P_2 – P_0 element performs well only in the Stokes region.

Tables 2 and 3 show the convergence results of the weak Galerkin method with the degree of polynomial $k = 1$ for $a = 1$ and $a = 10^4$, respectively. For both the small and large permeability cases, the convergence rate using $\|\cdot\|$ and L^2 -norm of the velocity \mathbf{u} are one and two, respectively, meanwhile the convergence rate of the pressure p in L^2 -norm is one as predicted in Lemma 3.3. This means that the weak Galerkin method is a stable and efficient algorithm in both Stokes and Darcy regions.

Example 5.2. Set the permeability $\kappa(\mathbf{x}, \omega) \equiv 1$ and the stochastic jump viscosity μ is specified as

$$\mu(x, \omega) = \begin{cases} 10^{-2}, & x \in D_d, \\ 1, & x \in D_s. \end{cases} \quad (38)$$

Let $\mathbf{f} = ((2\pi(\pi - 1) + 1) \sin(\pi x) \sin(\pi y), (2\pi(\pi + 1) + 1) \cos(\pi x) \cos(\pi y))^T$ and $\mathbf{g} = (\sin(\pi x) \sin(\pi y), \cos(\pi x) \cos(\pi y))^T$ in the stochastic Brinkman equations (1)–(3).

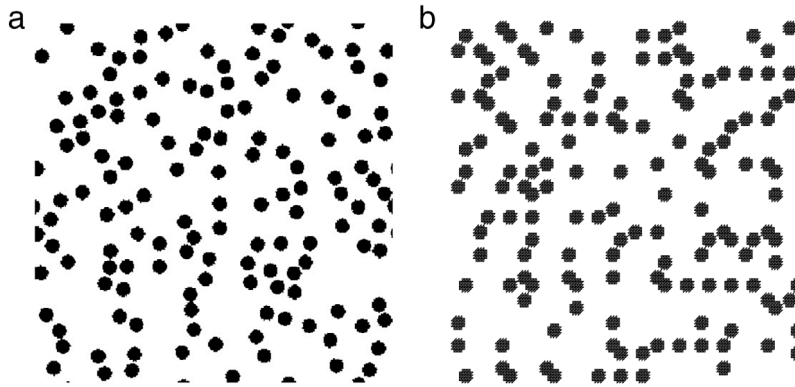


Fig. 2. Simulation of the stochastic jump coefficients: (a) the reference random media sample from [26] and (b) random media sample reconstructed by Lévy processes with $r = 0.2$.

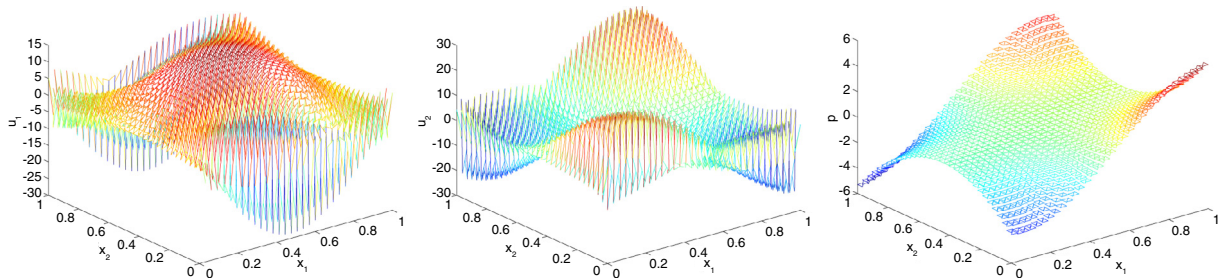


Fig. 3. The numerical solution of the deterministic Brinkman equation on the realization in Fig. 2b: first component of velocity u_1 (left), second component of velocity u_2 (middle), and pressure p (right).

For the simulation of the stochastic jump viscosity μ , we adopted a simulation method based on Lévy processes [26]. Let r be the ratio of the area of the Darcy region (black region) over the total area. Fig. 2a shows a real random media example taken from [27], where the white region and black region denote the Stokes and the Darcy regions, respectively. Fig. 2b is the sample reconstructed using the Lévy processes method with $r = 0.2$. Fig. 3 shows the numerical solution of the deterministic Brinkman equation on the realization in Fig. 2b. It is obvious that the velocity oscillate sharply near the interface of two materials, which needs huge degree of freedoms to capture the oscillation by standard FEM or even adaptive FEM.

In order to exhibit the efficiency of the WG method for capturing the oscillation of the solution near the interface of two regions, the multi-level Monte Carlo finite element method (MLMCFEM) and MLMCWG are implemented in this example.

In the simulation of these two methods, we adopt the coarsest stepsize $h_0 = 1$ and choose the maximal level $L = 6$ with $h_l = h_0/2^l$ for $l = 1, \dots, 6$. We also use the solution of the MCWG method with $h = \frac{1}{128}$ and $M = 10^6$ as the finest numerical solution to approximate $\mathbb{E}[\mathbf{u}]$ and $\mathbb{E}[p]$ in (29) and (34) since it is impossible to obtain an explicit expression for exact \mathbf{u} and p . For the multi-level Monte Carlo technique, according to Remark 4.5, we have huge number of deterministic PDEs on the coarse grid but the corresponding d.o.f. is small, and moreover, the number of deterministic PDEs on the fine grid is small which accelerated the overall computation.

Fig. 4 shows the convergence rate of MLMCFEM (4a) and the MLMCWG method (4b) for the stochastic Brinkman equations (1)–(3) with $r = 0.05$. The x -axes denotes the spatial stepsize h , while y -axes denotes the error. From this figure, we see that for the MLMCWG method, the convergence rate of $\|e_{u_h}\|$ and $\|e_{u_h}\|$ are one and two, respectively, meanwhile the convergence rate of $\|e_{p_h}\|$ is one as predicted in Theorem 4.3 and Proposition 4.4. But for the MLMCFEM, the corresponding errors do not converge as expected due to the low regularity of exact solution near the interface of two regions.

Example 5.3. Let the viscosity μ , \mathbf{f} and \mathbf{g} be the same as in Example 5.2, and the permeability $\kappa^{-1}(\mathbf{x}, \omega)$ is a lognormal random field, that is

$$\kappa^{-1}(\mathbf{x}, \omega) = \exp(c(\mathbf{x}, \omega)),$$

where c is a Gaussian field on D and $c(\mathbf{x}, \omega) \in L^\infty(D, \Omega)$. We test the performance of the single-level MCWG method and the MLMCWG method on the above problem.

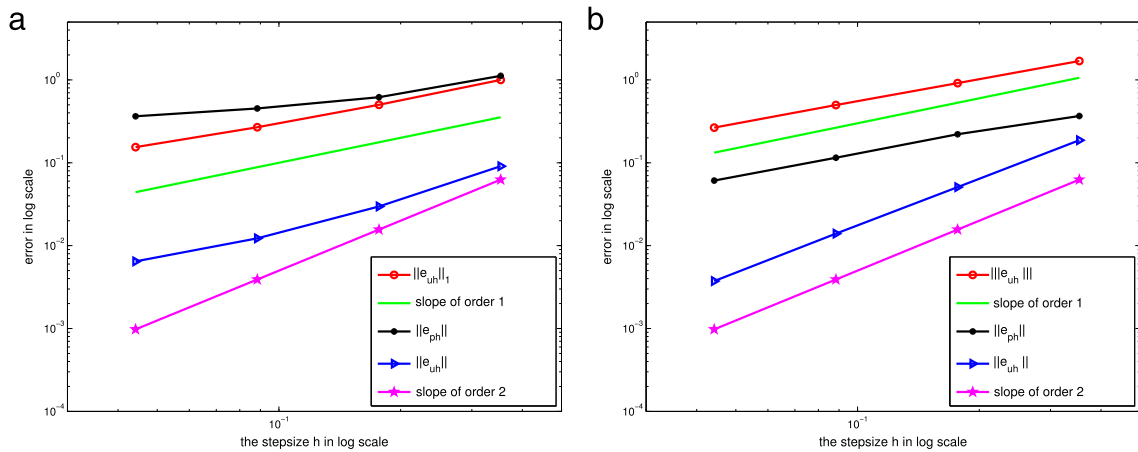


Fig. 4. Convergence rates of MLMCFEM (left) and MLMCWG method (right) with $r = 0.05$.

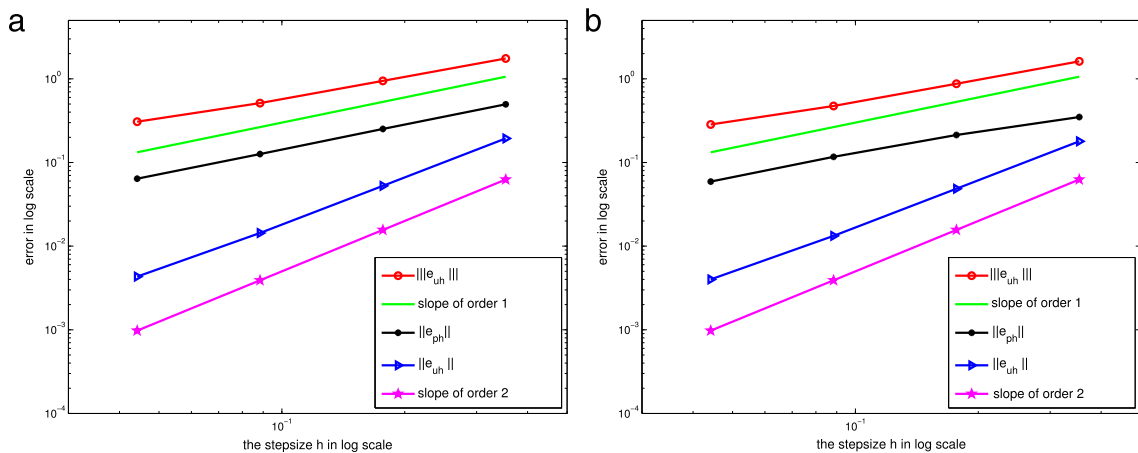


Fig. 5. Convergence rates of single-level MCWG method (left) and MLMCWG method (right) with $r = 0.05$.

Fig. 5 shows the convergence rate of the single-level MCWG method and the MLMCWG method with respect to the $\|e_{uh}\|$, $\|e_{uh}\|$, and $\|e_{ph}\|$ errors for the above stochastic Brinkman equations. It is easy to see that the convergence rate of $\|e_{uh}\|$ and $\|e_{uh}\|$ are one and two, respectively, meanwhile $\|e_{ph}\|$ is convergent of order one that is as predicted in Theorem 4.3 and Proposition 4.4, which means the computational results of MLMCWG is comparable to the single-level MCWG. However, it follows that the MLMCWG method is faster and more efficient than the single-level MCWG method since for the same h , MLMCWG requires to solve much smaller number of equations. The CPU time of these two methods listed in Table 4. The numerical solution of the MLMCWG method for the first and the second components of the velocity, and the pressure are shown in Fig. 6.

6. Conclusion

In this paper, we present an efficient MLMCWG method for solving stochastic Brinkman equations, which is stable for both Darcy's region and Stokes' region. With weak gradient operator and a stabilizer at hand, the weak Galerkin (WG) can capture the oscillation near the interface of two regions with high accuracy for each realization. The multi-level Monte Carlo (MLMC) technique balances the sampling error and the spatial approximation error, where the computational cost can be sharply reduced. The error estimates of the MLMCWG method for the velocity \mathbf{u} and pressure p are derived in terms of the spatial meshsize and the number of samples, meanwhile under the strategy (35), we obtain the optimal convergence of the approximate solutions with log-linear complexity. The numerical simulations are shown to verify the efficiency and robustness of the MLMCWG method.

Table 4

The comparison of CPU time for single-level MCWG method and MLMCWG method with $r = 0.05$, unit: second.

Level	CPU time	
	SLMCWG	MLMCWG
2	0.706E0	0.700E−3
3	1.634E1	0.980E−2
4	2.315E1	1.133E0
5	1.865E2	1.584E1
6	1.631E4	0.500E2

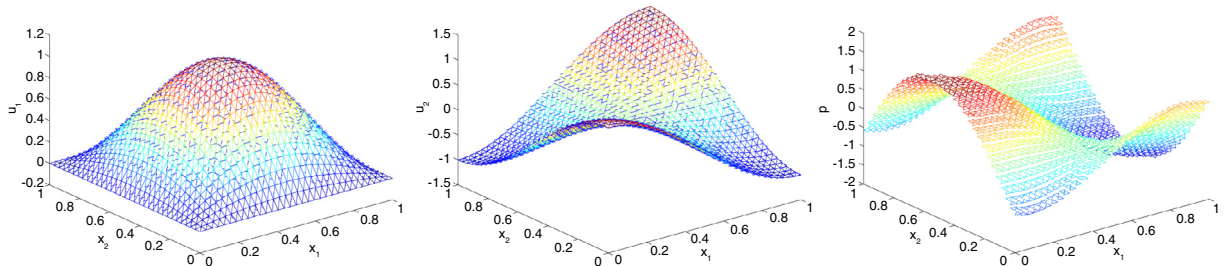


Fig. 6. The numerical solution of MLMCWG method: first component of velocity u_1 (left), second component of velocity u_2 (middle), and pressure p (right).

Acknowledgments

This work was supported by the National Natural Science Foundation of China (No. 11471141), the basic research of the science and technology development program of Jilin province (No. 20150101058JC). They also wish to thank the high performance computing center of Jilin university and computing center of Jilin province for essential computing support.

References

- [1] P. Popov, G. Qin, L. Bi, Y. Efendiev, R. Ewing, Z. Kang, J. Li, Multiscale methods for modeling fluid flow through naturally fractured carbonate karst reservoirs, in: Proceedings of the SPE Annual Technical Conference and Exhibition, SPE 110778, 2007.
- [2] V. Girault, P.A. Raviart, Finite Element Methods for Navier–Stokes Equations: Theory and Algorithms, in: Springer Series in Computational Mathematics, Springer-Verlag, 1986.
- [3] P. Angot, Analysis of singular perturbations on the Brinkman problem for fictitious domain models of viscous flows, Math. Methods Appl. Sci. 22 (1999) 1395–1412.
- [4] K. Mardal, D. Tai, R. Winther, A robust finite element method for Darcy–Stokes flow, SIAM J. Numer. Anal. 40 (2002) 1605–1631.
- [5] S. Badia, R. Codina, Unified stabilized finite element formulations for the Stokes and the Darcy problems, SIAM J. Numer. Anal. 47 (2009) 1971–2000.
- [6] J. Konno, R. Stenberg, $H(\text{div})$ -conforming finite elements for the Brinkman problem, Math. Models Methods Appl. Sci. 11 (2011) 2227–2248.
- [7] L. Mu, J. Wang, X. Ye, A stable numerical algorithm for the Brinkman equations by weak Galerkin finite element methods, J. Comput. Phys. 273 (2014) 327–342.
- [8] Y.Z. Cao, M. Gunzburger, X.M. He, X.M. Wang, Parallel, non-iterative, multi-physics domain decomposition methods for time-dependent Stokes–Darcy systems, Math. Comp. 83 (2014) 1617–1644.
- [9] Y.Z. Cao, F. Hua, M. Gunzburger, D.M. Wang, W.D. Zhao, Finite Element Approximations for Stokes–Darcy Flow with Beavers–Joseph Interface Conditions, SIAM J. Numer. Anal. 47 (2010) 1617–1644.
- [10] F. Müller, J. Patrick, D.W. Meyer, Multilevel Monte Carlo for two phase flow and Buckley–Leverett transport in random heterogeneous porous media, J. Comput. Phys. 250 (2013) 685–702.
- [11] T. Arbogast, H.L. Lehr, Homogenization of a Darcy–Stokes system modeling vuggy porous media, Comput. Geosci. 10 (2006) 291–302.
- [12] L. Mu, J.P. Wang, Y.Q. Wang, X. Ye, A computational study of the weak Galerkin method for second-order elliptic equations, Numer. Algorithms 63 (2013) 753–777.
- [13] J. Wang, X. Ye, A weak Galerkin finite element method for second-order elliptic problems, J. Comput. Appl. Math. 241 (2013) 103–115.
- [14] J. Wang, X. Ye, A weak Galerkin mixed finite element method for second-order elliptic problems, Math. Comp. 83 (2014) 2101–2126.
- [15] J.C. Zhang, K. Zhang, J.Z. Li, Z.B. He, A Weak Galerkin method for diffraction gratings, Appl. Anal. 96 (2) (2017) 190–214.
- [16] A. Barth, C. Schwab, M. Zollinger, Multi-level Monte Carlo finite element method for elliptic PDEs with stochastic coefficients, Numer. Math. 1 (2011) 123–161.
- [17] M. Giles, Improved multilevel Monte Carlo convergence using the Milstein scheme, in: Monte Carlo and Quasi-Monte Carlo Methods 2006, Springer, Berlin, 2008, pp. 343–358.
- [18] C.J. Gittelsohn, J. Konno, C. Schwab, R. Stenberg, The multi-level Monte Carlo finite element method for a stochastic Brinkman problem, Numer. Math. 125 (2013) 347–386.
- [19] S. Mishra, C. Schwab, J. Sukys, Multi-Level Monte Carlo finite volume methods for uncertainty quantification of acoustic wave propagation in random heterogeneous layered medium. SAM report No. 2014-22.
- [20] L. Mu, J. Wang, X. Ye, Weak Galerkin finite element method on polytopal mesh, Inter. J. Numer. Anal. Model. 12 (2015) 31–53.
- [21] P.S. Koutsourelakis, G. Deodatis, Simulation of multidimensional binary random fields with application to modeling of two-phase random media, J. Eng. Mech. ASCE 132 (2006) 619–631.

- [22] J.S. Li, X.S. Wang, K. Zhang, Multi-level Monte Carlo weak Galerkin method for elliptic equations with stochastic jump coefficients, *Appl. Math. Comput.* 275 (2016) 181–194.
- [23] R.E. Caflisch, Monte Carlo and quasi-Monte Carlo methods, *Acta Numer.* 7 (1998) 1–49.
- [24] Y.Z. Cao, R. Zhang, K. Zhang, Finite element and discontinuous Galerkin method for stochastic Helmholtz equation in R^d , *J. Comput. Math.* 26 (2008) 702–715.
- [25] J. Willems, Numerical upscaling for multiscale flow problems. Ph.D. thesis, 2009.
- [26] O.E. Barndorff-Nielsen, T. Mikosch, S.I. Resnick, *Lévy Processes: Theory and Applications*, Birkhäuser, Boston, 2001.
- [27] C.L.Y. Yeong, S. Torquato, Reconstructing random media, *Phys. Rev. E* 57 (1998) 495–506.